Nuclear Instruments and Methods in Physics Research A 1072 (2025) 170187

Contents lists available at ScienceDirect

Nuclear Inst. and Methods in Physics Research, A

journal homepage: www.elsevier.com/locate/nima

Full Length Article

A novel FPGA-based data acquisition for high-precision asymmetry measurements at low rates in electron scattering

A. Esser [a,*], A. Del Vincio [b,1], L. Doria [a], M. Hoek [a], F. Keil [a], N. Kozyrev [a], H. Merkel [a], M. Mihovilovič [d,e], U. Müller [a], J. Pochodzalla [a], B.S. Schlimme [a], T. Shao [a,c], S. Stengel [a], M. Thiel [a], C. Sfienti [a]

[a] Institut für Kernphysik, Johannes Gutenberg-Universität Mainz, D-55099 Mainz, Germany
[b] Department of Physics, Università di Pisa, 56126 Pisa, Italy
[c] Key Laboratory of Nuclear Physics and Ion-beam Application (MOE), Institute of Modern Physics, Fudan University, Shanghai 200433, China
[d] Jožef Stefan Institute, SI-1000, Ljubljana, Slovenia
[e] Department of Physics, University of Ljubljana, SI-1000, Ljubljana, Slovenia

ARTICLE INFO

Keywords:
Electron scattering
Asymmetry measurement
Polarized electron beam
Data acquisition electronics
FPGA

ABSTRACT

Asymmetry measurements in the scattering of polarized electrons on unpolarized targets are powerful tools to study the neutron distribution in nuclei and the multi-photon exchange contribution to the scattering process. Measuring these quantities requires not only precise counting of the scattered electrons, but also simultaneous accurate monitoring of the primary beam in order to correct any non-physical asymmetries. For this purpose, a dedicated data acquisition set-up was developed using FPGAs and fast discriminators for electron counting and voltage-to-frequency converters for beam monitoring. The performance of the new set-up was evaluated in experiments at the Mainz Microtron.

1. Motivation

When polarized electrons are scattered on unpolarized targets, two different types of asymmetries can be observed, depending on the orientation of the polarization vector. If the polarization vector points longitudinally, a parity-violating asymmetry (A_{PV}) occurs, which allows one to measure the weak form factor of the nucleus, a quantity closely related to the spatial distribution of neutrons in the nucleus [1]. In the case of a polarization vector normal to the scattering plane, the so-called beam-normal single spin asymmetry (A_n) arises, which is a probe for the multi-photon exchange amplitude [2–4]. Usually, A_n is an order of magnitude larger than A_{PV}, and therefore constitutes an important background to these measurements.

The A1 Collaboration [5] has performed several measurements of A_n at the Mainz Microtron (MAMI) [6] to systematically study the Q^2 dependence on ^{12}C [7] as well as its charge dependence (^{12}C, ^{28}Si, ^{90}Zr) [8]. Although these results are consistent with existing theoretical calculations, there is a significant disagreement between the value for A_n of ^{208}Pb measured by the PREX collaboration [9,10] and those calculations. This discrepancy called for an extension of the measurements in Mainz to heavier targets up to lead, using the same four momentum transfer ($Q^2 = 0.04\,\mathrm{GeV}^2/\mathrm{c}^2$) as for lighter nuclei to maximize the comparability. However, using lead as a target at these kinematics results in a significantly lower rate of elastically scattered electrons.

The previously used data acquisition system was originally designed for the readout of very high-rate luminosity monitors for the A4 experiment [11]. For this reason, analog integrators were used for the detector readout. This method worked well for light nuclei, however, as can be seen in Fig. 1, for the low rate on a lead target, the resolution of that DAQ[2] system was the limiting factor for a precise measurement.

To overcome these limitations, a new DAQ system was designed specifically to cope with low-rate signals. At the same time, this system must monitor various beam parameters that affect the measured asymmetry and control the sign of the electron beam polarity, as well as fast beam steering magnets required to distribute the heat load on the target. Ultimately, it was important to ensure that none of these tasks adversely affects the measurement.

While this system was tailored to the needs of the described experiments, it could be adapted as a small-scale low-cost data acquisition system for similar measurements such as in beam polarimeters.

* Corresponding author.
E-mail address: esser@uni-mainz.de (A. Esser).
[1] Now at University of Brescia, Italy
[2] Data Acquisition

https://doi.org/10.1016/j.nima.2024.170187
Received 30 September 2024; Received in revised form 2 December 2024; Accepted 24 December 2024
Available online 31 December 2024

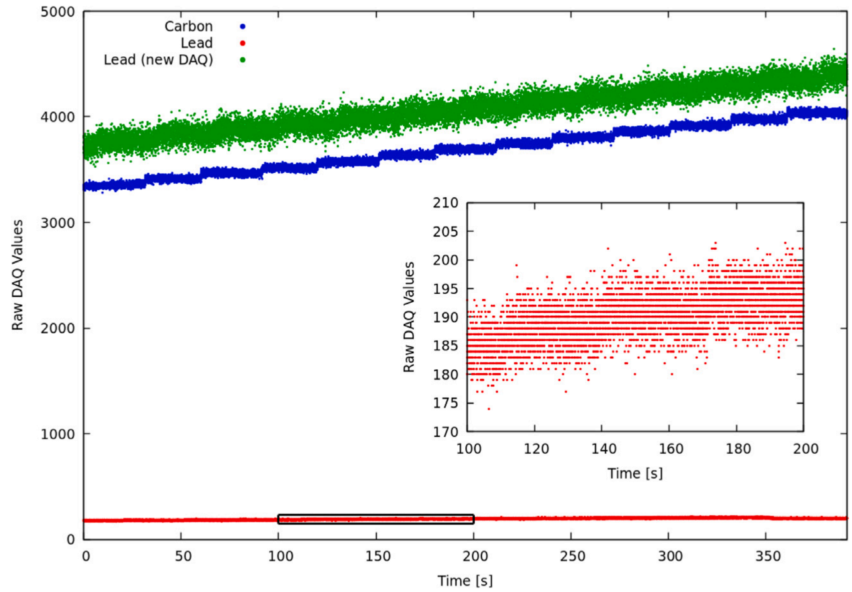

Fig. 1. Raw detector data read out with the old DAQ set-up. The channel with the highest rate is shown while the beam current is being ramped up from 17.75 μA to 20.75 μA in discrete steps. In blue (middle curve), a measurement on a carbon target is shown, red (lowest curve) shows a measurement on lead. The insert shows a zoomed section indicated by the black box. As a preview, the actual counts for lead in the integration window, measured with the new electronics are shown in green (uppermost curve).

2. Experimental set-up

For the previous measurements at MAMI, a polarized continuous wave electron beam, with an energy of 570 MeV and a beam current of 20 μA, impinges on an unpolarized solid target. The target thickness in this kind of experiments is chosen to be at most 1/10 of a radiation length of the target material to maximize the reaction rate and limit the beam depolarization due to multiple small-angle scattering. When A_n is measured, the polarization vector points up or down. For simplicity, "+" and "−" are used here to denote the different directions. A combination of a Mott polarimeter close to the beam source and a Møller polarimeter upstream of the target is used to measure and monitor the absolute degree of polarization and the direction of the polarization vector [12]. Two of the magnetic spectrometers of the A1 Collaboration (spectrometer A and B) are placed on opposite sides of the beam at forward angles. In the spectrometers, the elastically scattered electrons are focused on fused silica Čerenkov detectors. The radiators have the dimensions $300 \times 70 \times 10\,\mathrm{mm}^3$ ($100 \times 70 \times 10\,\mathrm{mm}^3$) for spectrometer A (spectrometer B), covering the elastic line in both spectrometers. They are read out with nine (three) quartz window PMTs,[3] labeled A0 to A8 (B0 to B2).

Data are acquired in time-slots of 20 ms (here referred to as sub-events), synchronized in length to the period of the power grid frequency. In this way any effect of 50 Hz power line noise, such as base line shifts, is identical for each sub-event, thus cannot introduce false asymmetries. Four consecutive sub-events, with polarity patterns "+ − −+" or "− + +−" are combined to form one so-called event. During each sub-event, the average PMT count rate is determined and values for various beam parameters are acquired, to calculate polarity correlated differences for each event. These values are:

1. The beam current measured close to the beam source (in the following indicated as I13) and upstream of the target (I21 and I21p). The latter is an offset-corrected higher resolution readout of the same beam monitor.
2. The beam energy (E18) measured in the last acceleration stage.
3. Multiple beam positions measured several meters upstream of the target (X21, Y21) and in close proximity to the target (X25, Y25, X26, Y26).

From these measurements, the position of the interaction point and the beam slope on the target are extrapolated.

The experimental asymmetry is calculated for each PMT from the counts in the two polarization states (N^+ and N^-):

$$A_{exp} = \frac{N^+ - N^-}{N^+ + N^-}. \tag{1}$$

The sign of the measured beam-normal asymmetry depends on which side the spectrometer is placed with respect to the electron beam.

To obtain the physical value A_{phys}, the experimental asymmetry needs to be corrected for asymmetries in the beam current (A_I) and for polarity correlated differences in the horizontal/vertical beam position (X/Y) and beam slope (X'/Y'), as well as in the beam energy (E). Finally, the result is divided by the absolute degree of beam polarization in the direction of the polarization component of interest (P).

$$A_{phys} = \frac{1}{P}\left(A_{exp} - c_I A_I - c_X \Delta X - c_Y \Delta Y - c_{X'} \Delta X' - c_{Y'} \Delta Y' - c_E \Delta E \right). \tag{2}$$

The correction factors ($c_I .. c_E$) are computed during the offline analysis by a multidimensional linear fit of the measured asymmetry against the measured polarity correlated differences. All values on the right side of Eq. (2) are subject to uncertainties. Ideally, the precision of the measurement is limited by the statistical uncertainty of the raw asymmetry (A_{exp}) which is of the order of 1×10^{-6}. The highest systematic error, of the order of 0.5×10^{-6}, is contributed by the uncertainty of the polarization measurement. This order of magnitude represents an upper limit for the desired uncertainty of the asymmetry measurement with the new DAQ system.

3. New data acquisition system

In order to increase the resolution for low-rate data, the overall concept of the readout electronics was changed from integrating the PMT current to counting individual pulses. Additionally, the new system uses voltage-to-frequency converters (VFCs) to acquire the beam parameters. A sketch of the newly developed electronics is depicted in Fig. 2. Four MYiR Z-turn boards [13] equipped with XILINX XC7Z020

[3] Photomultiplier Tube (ET Enterprises 9124QSB)

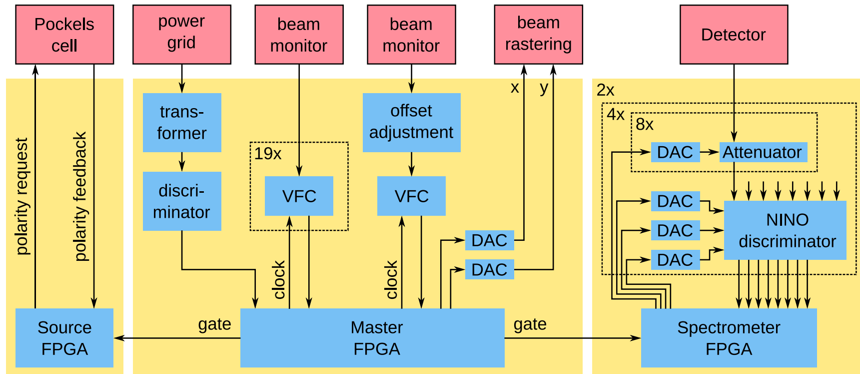

Fig. 2. Sketch of the new DAQ system. Existing components are shown in red, new ones in blue. The yellow boxes indicate the major parts of the set-up.

SoCs, here referred to as FPGAs,[4] form the backbone of the DAQ System. Each board is mounted onto a custom PCB[5] which provides the necessary in- and outputs. The detectors are read out by one FPGA each, which also controls the discriminator settings. One of the FPGAs is installed close to the beam source to control and monitor the Pockels cell, which changes the beam polarity. Finally, the master board generates the power grid synchronized gate signal and transmits it to the other FPGAs. This board also monitors the beam parameters and controls the fast beam rastering. All FPGAs are controlled and read out over ethernet by a custom software running on a PC outside of the experimental area.

Particular care was taken that there is no direct communication between the FPGAs other than the gate signals, and that these are galvanically isolated. This way, the information about beam polarity is only present on the board at the beam source and in the DAQ computer, minimizing the chance that this information has any influence on the detector readout by e.g. polarity correlated shifts in the ground level or the discriminator threshold, or polarity correlated variations in the gate length.

Master FPGA

The master FPGA is at the center of the DAQ system. It generates a master clock signal by dividing the FPGA clock of 100 MHz by an integer number, thus keeping it synchronous to the FPGA clock. The highest possible input frequency for the VFCs generated this way is 5.88 MHz. This clock signal is sent to all VFCs, which return a fraction of pulses depending on the measured voltage. The master clock signal is also used to define the readout gate length. For this purpose, the master FPGA is equipped with a fast discriminator, triggering on the zero-crossing point of an alternating low voltage synchronous to the power grid voltage. Between two rising edges of the alternating voltage, the number of pulses of the master clock is counted. At the beginning of an event, this number is fixed, and the gates are generated by counting the same number of clock cycles. This method assures that the readout gates for the four sub-events are identical in length, while keeping their length as close to the power grid period as possible to minimize the impact of 50 Hz power line noise. Two gates are separated by a gap of adjustable length, which was set to 68 μs for our running conditions. During this period, the data acquired in the last gate are read out and the beam polarity is reversed. The gate signal is used internally to read out the VFCs, and is sent to the spectrometer and source FPGAs. These signals are internally individually delayed such that all cable delays and beam transit times are compensated.

The reversal of the beam polarity introduces a small drop in beam intensity. Even though the majority of this is suppressed by the time gap between the readout gates, an influence of the polarity of the previous sub-event on the subsequent one is conceivable. Therefore a pseudo-randomly selected binary de Bruijn sequence [14] of order six is used to select the polarity patterns, assuring that all combinations of polarity patterns of subsequent events occur with the same frequency, thus minimizing any effect on the measured asymmetry.

Discriminator board

For the readout of the PMTs, a custom built PCB is used, which was originally manufactured for the readout of the A1 neutron polarimeter [15], but, due to its versatility, perfectly suits the needs of our detector readout. The board has 32 signal inputs, which are discriminated by four 8-channel NINO chips [16]. Since an identical threshold is set for all eight channels, the signals are beforehand attenuated using BAP64Q quad-pin diode attenuators. The threshold, attenuation, and further parameters, such as a hysteresis in the discriminator, and the output pulse length are set using DACs which are controlled by the FPGA. For the measurements with this set-up, the discriminator threshold was kept constant, while the individual signal attenuation was used for precise setting of the minimum accepted pulse height.

Voltage-to-frequency converters

The beam is monitored using specialized cavities and subsequent electronics, which generate voltage levels proportional to the individual beam parameters. Custom designed PCBs were manufactured using AD7741 VFCs to digitize these voltages. This chip can be driven with an external frequency, which allows one to run all VFCs with a synchronous frequency, thus eliminating phase drifts. In this mode, the VFCs return a fraction of the input clock pulses proportional to the measured voltage. This method of digitization has the benefit of intrinsically integrating the analog signals at much lower data rates as e.g. sampling ADCs. On the analog side of the PCBs, an adjustable passive voltage divider and a precision amplifier (AD8221) allow to match the range of the bipolar input signal to the unipolar VFC range.

Since the VFCs are mounted in close proximity to the beam monitor readout, the effect of analog noise is reduced to a minimum. Ground level differences between different parts of the accelerator are circumvented by optically decoupling the digital signals.

Most of the acquired beam parameters are proportional to the deviation from the nominal value. This is not the case for the beam current, where the voltage is proportional to the actual value. In order to increase the readout resolution for the beam current, one VFC is equipped with an adjustable offset voltage to shift the voltage for the nominal current to zero.

[4] Field Programmable Gate Array
[5] Printed Circuit Board

Beam rastering

For low melting point targets like lead and comparably high beam currents of 20 μA, it is mandatory to spread the associated heat load over a target area significantly larger than the beam spot. For this purpose, the beam line is equipped with two fast steering magnets, usually driven at frequencies in the range of 2 to 3 kHz. To prevent the beam rastering from introducing additional deviations of the average beam position between successive sub-events, the master board generates sinusoidal wave forms synchronized to the readout gates. In order to reduce the need for complex calculations by the FPGA, the wave function is pre-calculated and stored in lookup tables on the FPGA. During operation, the stored values are streamed to a fast SPI-DAC (LTC1655). Synchronicity with the readout gate is achieved by adjusting the update frequency of the DAC to the gate length.

4. Calibration

At the start of each experimental campaign, it is mandatory to set the global discriminator thresholds and individual attenuations for each PMT channel, and to adjust the offset voltage for the beam current readout. Additionally, calibration measurements need to be performed to relate the voltages measured with the VFCs to physical beam parameters in the offline analysis. Their dynamic voltage ranges are set beforehand and do not need adjustment. Frequent beam current scans are used to calibrate the beam current measurement and to correct for offsets in the PMT counts.

Discriminator thresholds

The correct setting of the discriminator threshold and signal attenuation is crucial. A very high threshold will result in a loss of statistics, but should not impact the measured asymmetry, while a very small threshold might lead to thermal PMT noise being picked up. Since this noise is unaffected by the beam polarity, this could cause a decrease in absolute value of the measured asymmetry. To obtain threshold values for all channels, the attenuation is varied over a large range, while other parameters of the experiment are kept constant. From the measured rate of PMT pulses, a pulse height spectrum can be derived as shown in Fig. 3 for selected channels of both detectors.

The steep rise towards lower thresholds can be attributed to PMT noise, while the right peak comprises actual detector hits. For all channels of spectrometer B (Fig. 3, bottom panel), a clear minimum is visible, which was selected as threshold value. The magnetic optics of this spectrometer focuses all elastically scattered electrons onto one point in the center of the radiator, leading to an equal distribution of the Čerenkov light onto all connected PMTs. In the case of spectrometer A, the electrons are focused on a line spanning the width of the radiator, where the position along the line is correlated with the scattering angle. This leads to vastly different count rates and an uneven distribution of Čerenkov light across the radiator bar. For the highest count rate PMTs (A1 to A3), again a clear minimum is visible, the other PMTs show a shoulder next to the thermal noise peak, which still allows one to set a threshold on this plateau. The PMTs with the smallest rate (A6 and A7) exhibit no structure, which would have allowed to define a proper threshold. These channels were henceforth dismissed from the analysis.

Beam monitor calibration

The beam position monitors are calibrated by using a pair of steering magnets upstream of the first monitor to slowly vary the beam position over wire targets, in horizontal and vertical direction, in a sawtooth pattern. The targets consist of three carbon rods each with a diameter of 0.5 mm with an average center-to-center distance of 1.18 mm, which are either arranged horizontally or vertically. When the rate in one of the PMTs is plotted versus the measured voltage in the monitor readout, distinct peaks, corresponding to the target wires, are visible. From the peak centers and the geometrically determined beam position in the monitor, a linear calibration function is then calculated.

Fig. 4 shows an example of the measured rate in PMT A1 for the calibration run plotted versus the calculated beam position on the target, after the calibration was performed. The vertical lines show the center positions of the three carbon rods used for calibration, which are in good agreement with the peaks in count rate. The single points spread out in the lower region correspond to events during which the beam is quickly reset to the starting position.

The beam energy monitor measures path length variations of the electron beam through one bending magnet in the last accelerator stage, where the bending radius and therefore the path length is proportional to the beam energy. For this purpose, the phase of the electron beam is measured with two cavities before and after this magnet. The high frequency signals from both cavities are combined in an analog frequency mixer and subsequently low-pass filtered to obtain an analog voltage signal proportional to the phase difference between the cavities, and therefore to beam energy variations. Since the beam energy monitor is already calibrated, it is sufficient to superimpose a signal onto the voltage, which matches a defined energy variation.

Detector calibration

The measurement of the beam current and the offset counts of the PMTs are calibrated in a procedure conducted every three hours. Therefore, the beam current is varied in discrete steps around the nominal value. The voltage measured at the beam current monitors and the counts of every PMT are then averaged over all events in one step. The average values are linearly fitted versus the beam current measured with a fluxgate current probe which is already calibrated, but lacks the bandwidth to resolve variations in beam current of the order of the readout gate length. For the calibration of the beam current measurement, an offset and a scale factor are extracted from the fit. In the case of the PMTs, only the offset is needed for the further analysis.

5. Performance evaluation

The performance of the new set-up was tested using ^{12}C and natural lead targets. These test measurements are limited in statistics but show that the new DAQ system works as intended.

VFC resolution

During commissioning, the average power grid frequency was 50.005 Hz with a standard deviation of 25 mHz. This corresponds to 117 635 cycles of the master clock (standard deviation 59 cycles). The minimum (maximum) fraction of pulses returned by the VFCs is 0.05 (0.45), corresponding to the maximum negative (positive) input voltage. Therefore, the full range of the VFCs in this set-up corresponds to a variation of 47054 counts, leading to a trade-off between the maximum working range and the voltage resolution. The ranges are chosen such that the extreme conditions during the calibration procedures are fully covered, resulting in the resolutions given in Table 1. The output signal of the beam monitors is proportional to the beam current. Therefore, these values are only valid for a nominal beam current of 20 μA. Table 1 also contains the standard deviation of the measured parameters, showing that it is always larger than the resolution and significantly smaller than the selected range. The impact of the resolution on the asymmetry measurement is greatest for the position measurements, where the correction factors can be of the order of 50 ppm/μm, and smallest for the energy measurement, where the correction factor is of the order of 0.1 ppm/eV.

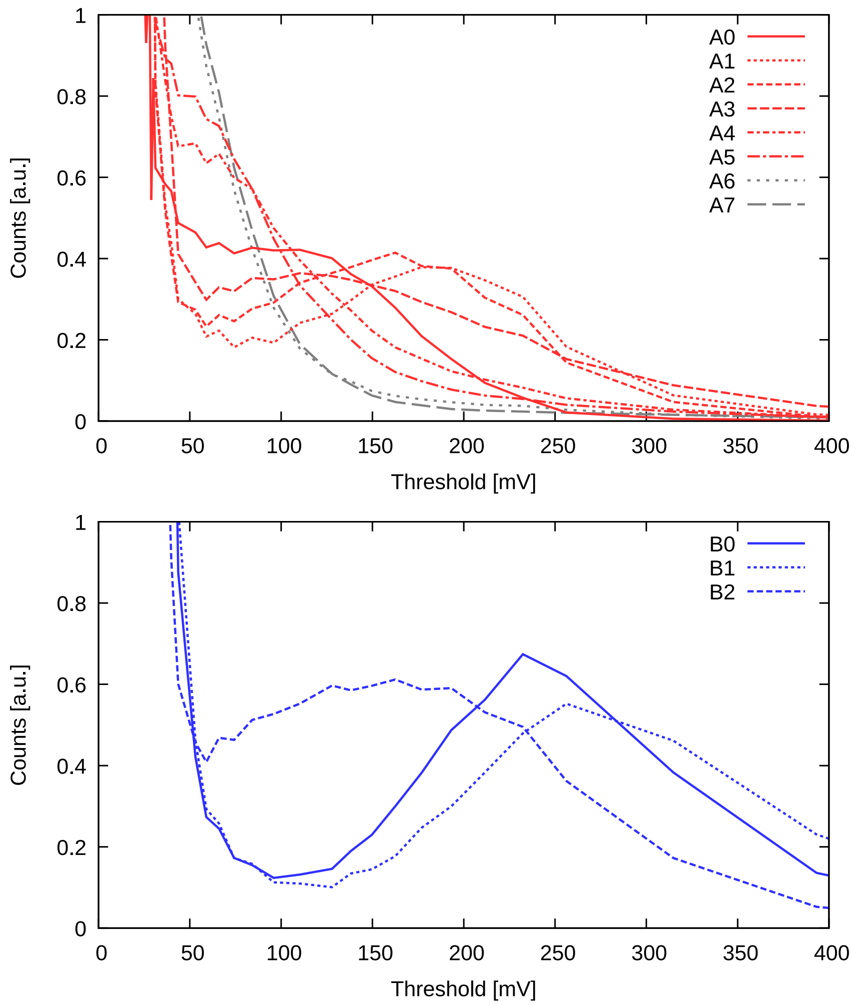

Fig. 3. Pulse height spectra of the individual PMT channels of the detectors placed in spectrometer A (top) and spectrometer B (bottom).

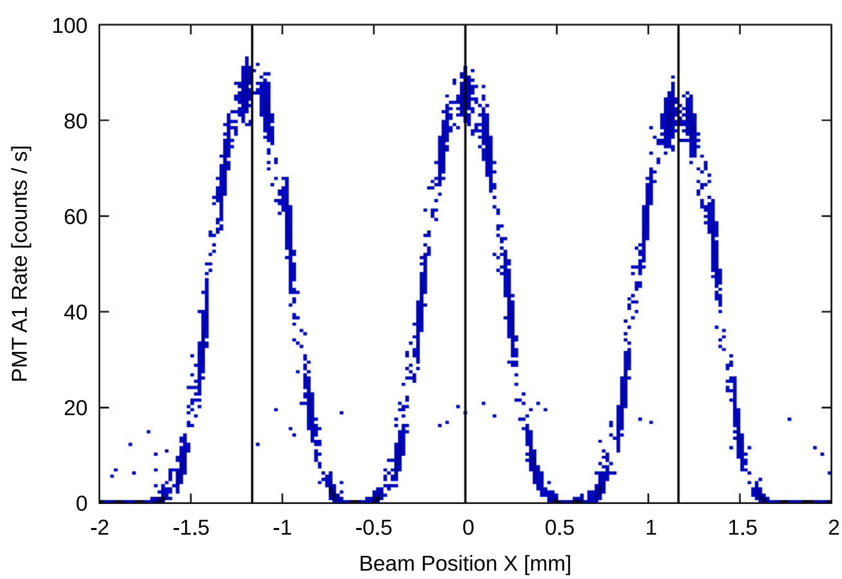

Fig. 4. Verification of the XY-monitor calibration. The detector rate in PMT A1 is shown versus the reconstructed beam position on the target. The vertical lines indicate the positions of the carbon rods in the calibration target.

Table 1
Ranges and resolutions of the VFC readout of the beam parameters for a beam current of 20 μA and a power grid frequency of 50 Hz. The rightmost column shows the standard deviation over the duration of the test experiment of the measured values for each parameter. Y26 is missing, since the analog electronics of this beam monitor were inoperative during the experiment.

Parameter	Range	Resolution	Standard deviation
I21	72.9 μA	1.55 nA	35.5 nA
I21p	4.92 μA	0.105 nA	35.1 nA
I13	69.1 μA	1.47 nA	31.5 nA
E18	122.9 keV	2.61 eV	358.5 eV
X21	6.08 mm	0.129 μm	699.4 μm
Y21	44.0 mm	0.936 μm	1630 μm
X25	9.72 mm	0.207 μm	151.5 μm
Y25	13.4 mm	0.285 μm	170.0 μm
X26	44.1 mm	0.937 μm	123.9 μm

VFC precision

In order to evaluate the precision of the beam monitoring system, identical values can be measured using different VFCs. This was done in a measurement with a constant voltage source, as well as by comparing beam parameters measured at different positions. The result of the constant voltage measurement is shown in Fig. 5. Here, an AA battery was connected to both channels of a VFC with a range of U_R = 8 V (±4 V). The average difference of 39.97 mV can be attributed to production tolerances in the internal voltage dividers used to adjust the range. The standard deviation of the distribution is $\sigma_U = 151\,\mu\mathrm{V}$. Dividing this value by $\sqrt{2}$ yields the absolute precision of one VFC (107 μV), which can then be expressed as a relative precision of:

$$\delta_U = \frac{\sigma_U}{\sqrt{2}U_R} = 1.33 \cdot 10^{-5}. \quad (3)$$

To estimate the precision of the beam readout, one can compare the values for identical beam parameters measured by different components. For the beam energy, this is not possible, since it is only read out by one system. The beam current is measured at two independent points along the beam line, one close to the source and one just upstream of the target. The difference of both measurements for two weeks of measurement time is shown in Fig. 6. The non-zero average value (3.08 nA) can be explained by slight variations in the calibration, as well as by beam losses in the accelerator. The width of the distribution (σ = 29.2 nA) can serve as an upper bound for the precision of both monitors. However, only for the beam monitor close to the target, the voltage is shifted to 0 V for the nominal beam current, which significantly increases its resolution. Additionally, the beam current asymmetry is being minimized for this point in the beam line. Therefore, this measurement is far more reliable than the measurement close to the beam source, making a comparison difficult.

The beam position is measured at three locations: 8.28 m (X21), 1.28 m (X25) and 0.78 m (X26) upstream of the target. There are no beam line magnets between these locations. This allows one to evaluate the precision of the beam position measurement by comparing the polarity correlated beam position difference (ΔX) calculated by a geometric interpolation from the outer position monitors to the value measured in the central cavity. Due to a defect in the analog electronics of the beam monitor Y26, this method is only applicable for the horizontal direction. The result of this comparison is shown in Fig. 7. The variation of this distribution (4.80 μm) serves as an upper bound for the precision of individual measurements. The impact of the position measurement error on the resulting asymmetry can be estimated from the average value of the distribution (0.001 μm). Using the position correction factor $c_X = 32.5 \times 10^{-6}\,\mu\mathrm{m}^{-1}$ obtained with the multidimensional fit for spectrometer A, this translates to an asymmetry error of only 0.032×10^{-6}. This is significantly smaller than the statistical uncertainty of 4.0×10^{-6} for this data set.

Linearity

For the beam current dependence, the aforementioned calibration measurements can be used to assess the linearity. In the calibration procedure, a linear fit of the count rate of each PMT over the beam current is performed. Assuming a linear behavior, the residuals should be distributed evenly around zero for the entire calibration range. Fig. 8 shows the distribution of residuals normalized to the count rate for 30 different calibrations of the highest rate PMT A1. The red error bars show the average value for each current step and the standard deviation of the distribution. The largest difference of average values of consecutive steps can be seen between beam currents of 19.75 μA and 20 μA. To calculate an upper bound of the impact of this non-linearity on the asymmetry, the calibration function was modified to conform to this difference. This resulted in a variation of the asymmetry of ≈ 2%. Using the value of A_n published in [7] for ^{12}C at $Q^2 = 0.04\,\mathrm{GeV}^2/c^2$ as a reference, this would amount to $\Delta A_n = 0.5 \times 10^{-6}$.

As an example of the impact of other parameters on the measured asymmetry, Fig. 9 shows the uncorrected asymmetry for PMT A1 versus the polarity correlated difference in the horizontal beam position. This is the parameter which causes the highest asymmetry correction apart from the beam current. Most of the data are concentrated at small position differences < 3 μm with no visible correlation with the measured asymmetry. For a small fraction of events, larger differences of the order of tens of micrometers are measured. The most likely cause of these events are adjustments of the stabilization system for the absolute beam position and current, which happen every 10 s. As can be observed, the statistical variation of the asymmetry far exceeds the impact of beam fluctuations. The total correction due to polarity correlated differences in the horizontal position for this PMT amounts to 0.017×10^{-6}. This shows that even for the beam parameters with the strongest impact on the measured asymmetry, linear corrections are feasible, and that they contribute minimally to the systematic uncertainty.

Rate deficiency

The highest recorded PMT rate for a beam current of 20 μA on a lead target was of the order of $6 \times 10^5\,\mathrm{s}^{-1}$, corresponding to 12 000 pulses per sub-event. The nominal pulse length in the test measurements was 30 ns, making it impossible to resolve subsequent pulses with a time separation smaller than the pulse length. Using a Monte-Carlo simulation, the average loss of counts due to overlapping pulses was estimated to be 2% for this configuration. While this is a significant fraction of all events, the count rate, and therefore the loss of counts, is, apart from the measured asymmetry, independent of the beam polarity. Therefore, this effect only causes a loss of statistics, but has no relevant impact on the measurement result.

Gate length variation

Assuming a constant beam current, the average number of PMT counts is proportional to the gate length. Keeping the gate length constant during an event, reduces the effect of gate length fluctuations on the measured asymmetry. However, there is a near constant difference in the gate length measured in the FPGAs on the spectrometers compared to the master FPGA. The average difference is 48 ns (76 ns) for spectrometer A (B). The standard deviation of this difference is less than the resolution of the gate length measurement of 10 ns. A likely cause of this discrepancy are small variations of the individual FPGA clock speeds. Since the beam polarity and the gate signals are independently created, they are not correlated. The FPGA with the largest polarity correlated length variation was the one at the beam source with a relative variation of less than 10^{-9}. The differences in gate length could have been reduced by synchronizing the 100 MHz clocks of the different FPGAs, but this would have introduced more complexity for marginal gains.

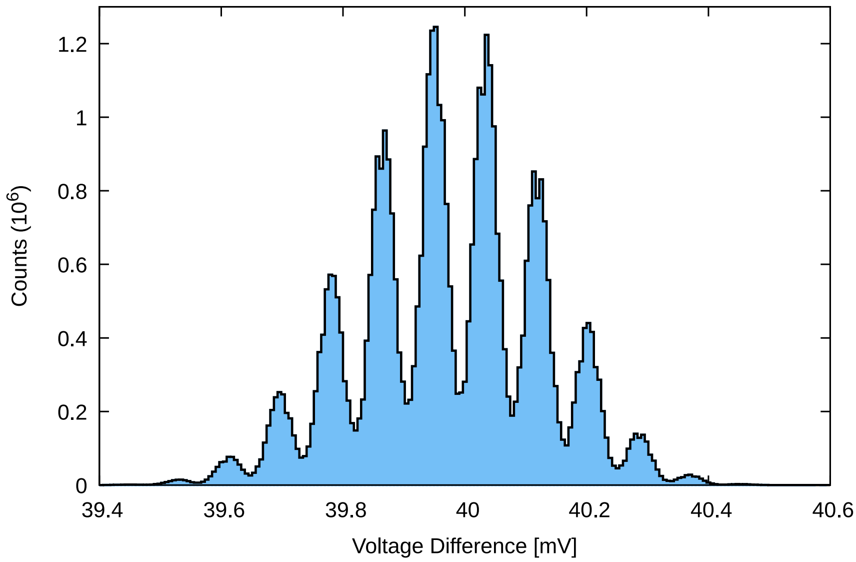

Fig. 5. Voltage difference between two VFC channels with identical ranges of ±4 V, measuring the same constant input voltage. The individual peaks correspond to discrete numbers of counts in the integration window, which are broadened by fluctuations in the gate length due to changes in the power grid frequency. The data were acquired over a time period of 10 days.

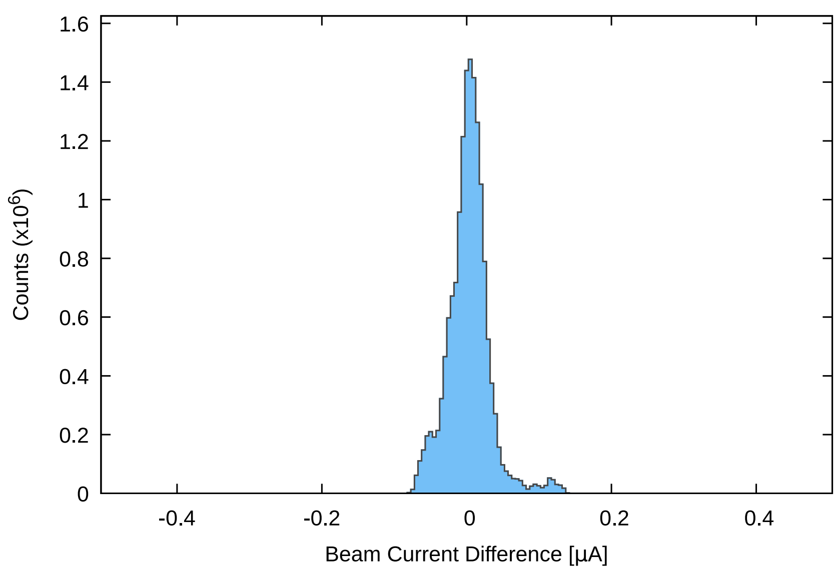

Fig. 6. Difference of the beam current measurements with the current monitor close to the source (I13) and the one close to the experiment (I21p).

Asymmetry measurement

The main objective of the new set-up is to measure A_n on a ^{208}Pb target. For better comparability with previous results, and to make use of the higher counting rate, ^{12}C was chosen as a target for a benchmark measurement. Beam energy and spectrometer angle, which define the Q^2 of the reaction, were set as close as possible to the values for the measurement published in [8]. In addition, a measurement using the same kinematics was performed on a natural lead target, which generates similar rates as isotopically enriched ^{208}Pb. Due to the isotopic composition of the target a direct comparison of the asymmetry with measurements on pure ^{208}Pb is not meaningful. To prevent any misinterpretation, a random offset was added to the data points for lead which are shown in Fig. 10 together with the measurement on ^{12}C and the previous results on carbon (gray bands). To make the plot more comprehensible, the asymmetry is shown, not corrected for the side on which the spectrometer is located. To obtain the physical value, the data for spectrometer B need to be inverted. The total measurement time was only 12 h (78 h) for ^{12}C (Pb), which explains the significantly larger statistical uncertainties compared to the previous data. It is noteworthy that the PMTs, though read out independently, are optically coupled to the same fused silica bar. Therefore, the individual measurements are not independent. This explains why the measured values are in better agreement than expected from the individual error bars. This is especially important in the case of spectrometer B, which focuses all electrons to one point in the detector. In the case of spectrometer A, the electrons are spread out on a line with the highest rate in front of PMT A1. For the lead target, the difference in rate is much more pronounced due to the forward peaking of the cross section, which explains the larger statistical errors for higher channel numbers in spectrometer A. The average asymmetry value for each spectrometer is calculated as a weighted mean of the asymmetries of each PMT channel. The absolute number of counts during the measurement in each channel is used as weighting factor. This way, each count has the same weight in the asymmetry result.

Even with the limited statistics, the acquired data on carbon are in agreement with previous results, proving the applicability of the novel

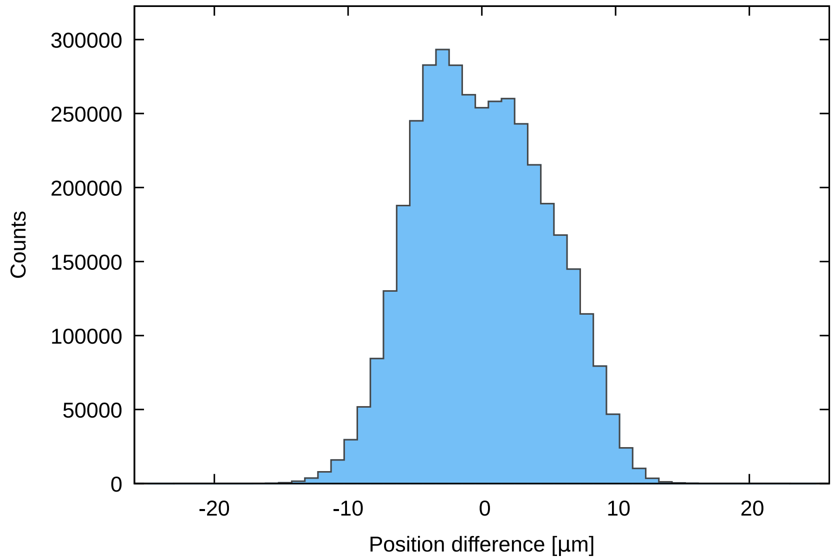

Fig. 7. Difference of the value measured in beam monitor X25 and the interpolated value from monitors X21 and X26. The parameter shown is the polarity correlated position difference (ΔX).

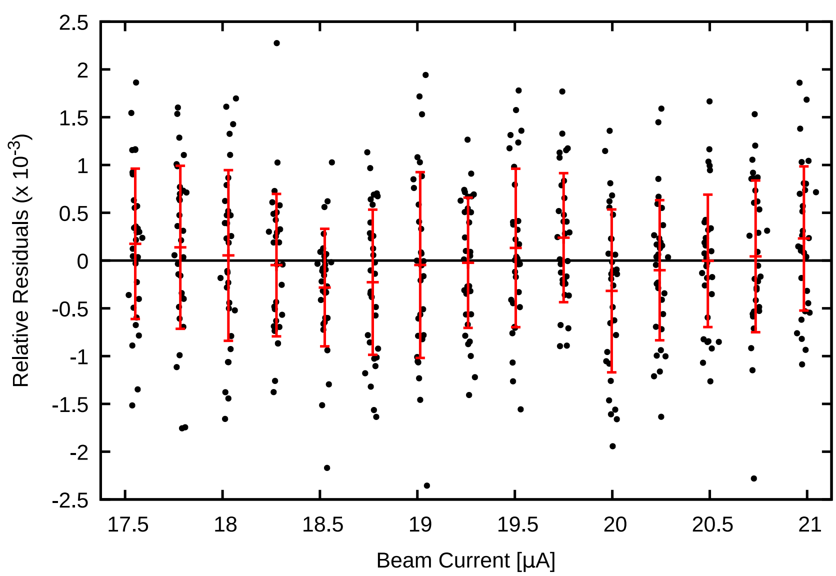

Fig. 8. Residuals divided by the count rate for PMT A1 for all calibration measurements (black points) as well as average value and standard deviation for every beam current division (red error bars).

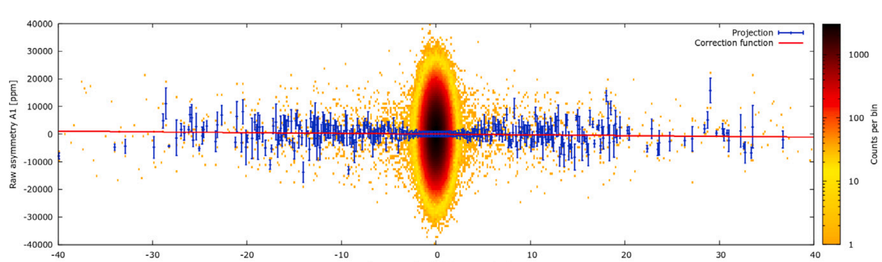

Fig. 9. Uncorrected asymmetry measured by PMT channel A1 over the polarity correlated difference in beam position. The red line shows the correction function obtained in the multiple linear regression.

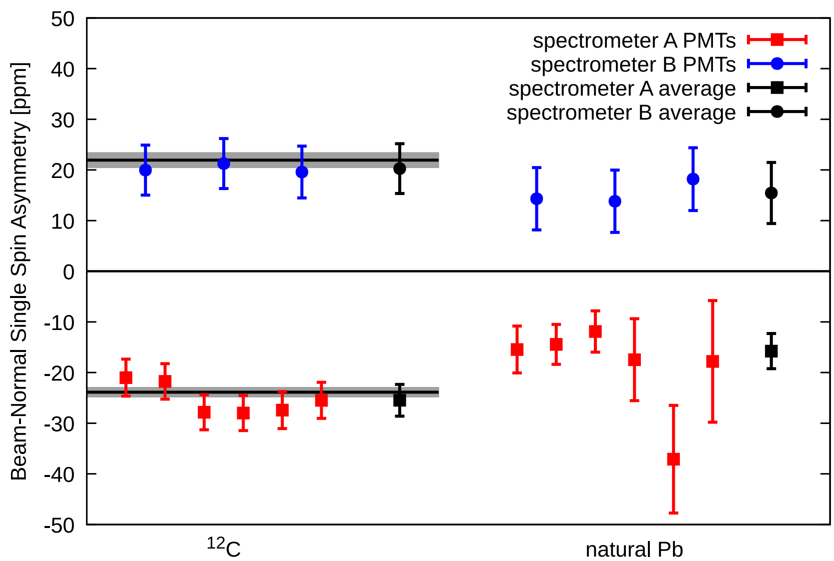

Fig. 10. Measured beam-normal single spin asymmetry for ^{12}C on the left and natural lead on the right at $Q^2 = 0.04\,\mathrm{GeV}^2/c^2$. To prevent possible misinterpretation, a random offset was added to the data points for lead. The gray bands show the result published in [7] (central value and statistical uncertainty), which comprises significantly higher statistics.

system to the intended measurement with a competitive uncertainty. Due to its modularity, it can be easily extended to different detector systems with larger number of channels, or more beam parameters to be monitored.

CRediT authorship contribution statement

A. Esser: Writing – review & editing, Writing – original draft, Visualization, Software, Methodology, Formal analysis, Conceptualization. **A. Del Vincio:** Software, Investigation. **L. Doria:** Investigation. **M. Hoek:** Writing – review & editing, Software, Methodology, Investigation. **F. Keil:** Investigation. **N. Kozyrev:** Investigation. **H. Merkel:** Software, Formal analysis, Conceptualization. **M. Mihovilovič:** Investigation. **U. Müller:** Writing – review & editing, Investigation. **J. Pochodzalla:** Investigation. **B.S. Schlimme:** Investigation. **T. Shao:** Investigation. **S. Stengel:** Writing – review & editing, Investigation. **M. Thiel:** Writing – review & editing, Resources, Project administration, Investigation. **C. Sfienti:** Writing – review & editing, Supervision, Project administration, Funding acquisition.

Funding

This work was supported by the PRISMA+ (Precision Physics, Fundamental Interactions and Structure of Matter) Cluster of Excellence, the Deutsche Forschungsgemeinschaft, Germany through the Collaborative Research Center 1044, the Deutsche Forschungsgemeinschaft, Germany through the individual grant No. 454637981, and the Federal State of Rhineland-Palatinate.

Declaration of competing interest

The authors declare that they have no known competing financial interests or personal relationships that could have appeared to influence the work reported in this paper.

Acknowledgment

We greatly appreciate the support from the MAMI operators, the accelerator group and the workshops, first of all the electronics department.

Data availability

Data will be made available on request.

References

[1] C.J. Horowitz, et al., Parity violating measurements of neutron densities, Phys. Rev. C 63 (2001) 025501, http://dx.doi.org/10.1103/PhysRevC.63.025501.
[2] A. De Rújula, et al., Elastic scattering of electrons from polarized protons and inelastic electron scattering experiments, Nuclear Phys. B 35 (2) (1971) 365–389, http://dx.doi.org/10.1016/0550-3213(71)90460-3.
[3] A.V. Afanasev, et al., Collinear photon exchange in the beam normal polarization asymmetry of elastic electron–proton scattering, Phys. Lett. B 599 (1) (2004) 48–54, http://dx.doi.org/10.1016/j.physletb.2004.08.023.
[4] M. Gorchtein, et al., Analyzing power in elastic scattering of electrons off a spin-0 target, Phys. Rev. C 77 (2008) 044606, http://dx.doi.org/10.1103/PhysRevC.77.044606.
[5] K. Blomqvist, et al., The three-spectrometer facility at the mainz microtron mami, Nucl. Instrum. Methods Phys. Res. A 403 (2) (1998) 263–301, https://doi.org/10.1016/S0168-9002(97)01133-9.
[6] A. Jankowiak, The mainz microtron MAMI –past and future, Eur. Phys. J. A 28 (1) (2006) 149–160, http://dx.doi.org/10.1140/epja/i2006-09-016-3.
[7] A. Esser, et al., First measurement of the Q^2 dependence of the beam-normal single spin asymmetry for elastic scattering off carbon, Phys. Rev. Lett. 121 (2018) 022503, http://dx.doi.org/10.1103/PhysRevLett.121.022503.
[8] A. Esser, et al., Beam-normal single spin asymmetry in elastic electron scattering off ^{28}si and ^{90}zr, Phys. Lett. B 808 (2020) 135664, http://dx.doi.org/10.1016/j.physletb.2020.135664.
[9] S. Abrahamyan, et al., New measurements of the transverse beam asymmetry for elastic electron scattering from selected nuclei, Phys. Rev. Lett. 109 (2012) 192501, http://dx.doi.org/10.1103/PhysRevLett.109.192501.
[10] D. Adhikari, et al., New measurements of the beam-normal single spin asymmetry in elastic electron scattering over a range of spin-0 nuclei, Phys. Rev. Lett. 128 (2022) 142501, http://dx.doi.org/10.1103/PhysRevLett.128.142501.
[11] F.E. Maas, Parity-violating electron scattering at the mami facility in mainz, Eur. Phys. J. A 17 (3) (2003) 339–343, http://dx.doi.org/10.1140/epja/i2002-10201-y.
[12] B. Schlimme, et al., Vertical beam polarization at mami, Nucl. Instrum. Methods Phys. Res. A 850 (2017) 54–60, https://doi.org/10.1016/j.nima.2017.01.024.
[13] Z-turn board, 2017, https://www.myirtech.com/download/Zynq7000/Z-turnBoard.pdf. (Accessed June 11 2024).
[14] N.G. de Bruijn, A combinatorial problem, Nederl. Akad. Wetensch. 49 (1946) 758–764.
[15] R. Spreckels, et al., A highly segmented neutron polarimeter for a1, Nucl. Instrum. Methods Phys. Res. A 1062 (2024) 169171, https://doi.org/10.1016/j.nima.2024.169171.
[16] F. Anghinolfi, et al., Nino: an ultra-fast and low-power front-end amplifier/discriminator asic designed for the multigap resistive plate chamber, Nucl. Instrum. Methods Phys. Res. A 533 (1) (2004) 183–187, Proceedings of the Seventh International Workshop on Resistive Plate Chambers and Related Detectors, https://doi.org/10.1016/j.nima.2004.07.024.